Available online at www.sciencedirect.com

ScienceDirect

www.elsevier.com/locate/jmbbm

Research Paper

Tribological properties of biocompatible Ti–10W and Ti–7.5TiC–7.5W

Myounggeun Choi[a], *Eunji Hong*[a], *Jungwon So*[b], *Seokbeom Song*[b], *Byoung-Suck Kim*[c], *Akiko Yamamoto*[d], *Yong-Suk Kim*[a], *Jinhan Cho*[e], *Heeman Choe*[a,*]

[a]*School of Advanced Materials Engineering, Kookmin University, 77 Jeongneung-ro, Seongbuk-gu, Seoul 136-702, Republic of Korea*
[b]*R&D Team, CG Bio Co., Sangdaewon-dong, Jungwon-gu, Seongnam-si, Kyunggi-do 462-807, Republic of Korea*
[c]*Department of Orthopedic Surgery, Daewoo General Hospital, 363 Dumo-dong, Geoje-si, Gyeongsangnam-do 656-711, Republic of Korea*
[d]*Biomaterials Unit, International Center for Materials Nanoarchitectonics, National Institute for Materials Science, 1-1 Namiki, Tsukuba, Ibaraki 305-0044, Japan*
[e]*Department of Chemical and Biological Engineering, Korea University, Anam-dong, Seongbuk-gu, Seoul 136-701, Republic of Korea*

ARTICLE INFO

Article history:
Received 15 September 2013
Received in revised form
14 November 2013
Accepted 21 November 2013
Available online 28 November 2013

Keywords:
Biocompatibility
Cell proliferation
Titanium
Wear mechanism

ABSTRACT

This study investigates and compares the microstructure, biocompatibility, and tribological properties of two different Ti-based composites, Ti–10W and Ti–7.5TiC–7.5W, with those of pure Ti for their potential use in biomedical applications. In particular, cold and hot isostatic-pressing and arc-melting methods were utilized and compared for the microstructure of the composites. Nano-scratch measurements and pin-on-disk wear tests were employed to understand their tribological behavior. As compared to pure Ti, Ti–10W and Ti–7.5TiC–7.5W showed significantly improved nano-scratch resistance (by 85 and 77%, respectively) and wear resistance (by 64 and 66%, respectively), in good agreement with hardness measurements. For biocompatibility examination, both micro-culture tetrazolium test (MTT) and water soluble tetrazolium (WST-1) test were used to quantify the cell viability of human osteoblasts and mouse fibroblasts on the materials. Both of the Ti-based composites showed acceptable biocompatibility in comparison with the pure Ti control.

© 2013 Elsevier Ltd. All rights reserved.

1. Introduction

In recent years, considerable attention has been paid to the development of new materials for implant applications such as replacement of damaged bones, teeth, or blood vessels because the anticipated average human lifespan is steadily increasing (Temenoff and Mikos, 2008; Geetha et al., 2009). What makes this area of research rather difficult is that very diverse types of materials are used for different implant applications, e.g., polymers for soft tissues and artificial lens, and strengthened metal alloys or ceramics for load-bearing

*Corresponding author. Tel.: +82 2 910 4417; fax: +82 2 910 4320.
E-mail address: heeman@kookmin.ac.kr (H. Choe).

1751-6161/$ - see front matter © 2013 Elsevier Ltd. All rights reserved.
http://dx.doi.org/10.1016/j.jmbbm.2013.11.014

joints (Geetha et al., 2009). In other words, the required mechanical/physical properties and biocompatibility can vary, depending on where and how the implant is used.

Compared to ceramics and polymers, metallic implant materials possess superior strength, fracture toughness, ductility, and machinability, despite their relatively low corrosion resistance; they have particularly low corrosion resistance in the basic environment of the human body (Enderle et al., 2005). Among a variety of metallic implant materials, pure Ti and Ti alloys are considered attractive solutions owing to the formation of the dense, thin TiO_2 film on the surface, giving rise to good corrosion resistance. In addition, the formation of TiO_2 on the surface of Ti alloys such as Ti–6Al–4V takes place in about 8 min, which is approximately 55% and 330% faster than the formation of oxide films on the surfaces of Co–28Cr–6Mo and 316L stainless steel in 0.9% saline solution, respectively (Geetha et al., 2009). Furthermore, with significantly less formation of fibrous soft tissue (e.g., approximately one-tenth that formed on the Co-based alloy (Brunette et al., 2001)), the formation of a direct bond is feasible between Ti or a Ti alloy and osseous tissue (Adell et al., 1970). The direct bond is strong and tough because it forms stable, biocompatible, and nontoxic $CaTiO_3$ by combining TiO_2 and Ca ions in the osseous tissue (Feng et al., 2004). Another main advantage of Ti and its alloys is their low stiffness, such that they are less likely to result in stress shielding than traditional implant materials such as stainless steels or Co alloys, which have a stiffness of 190–250 GPa (Ashby and Jones, 1987). Finally, Ti and its alloys have low magnetism and hence are safer for use with MRIs (Frank, 2002).

However, Ti and Ti alloys do not possess sufficient mechanical properties to be used as replacements in human body parts exposed to high levels of stress and wear, e.g., femoral heads for hip replacement. Efforts have been made to achieve the required mechanical properties through hardened Ti alloys or Ti composites reinforced with hard ceramic particles (Iijima et al., 2003), with limited success. This study thus reports a new hardening strategy by reinforcing Ti with additions of tungsten (W) and titanium carbide (TiC), and investigates their effects on the biological and tribological properties of Ti. We fabricated our samples using two different processing routes, which are cold and hot isostatic-pressing (CHIP) and arc-melting (AM) processes. We then compared the microstructure and properties of the samples fabricated by those two different processing routes. With the addition of W, a solid-solution Ti–W alloy is achieved, resulting in substantial strengthening, whereas with the addition of TiC, a Ti–TiC–W composite is achieved, resulting in a secondary reinforcement effect in terms of macrohardness.

2. Material and methods

2.1. Sample fabrication

Two different processing methods, namely, the combined cold and hot isostatic-pressing (CHIP) and arc-melting (AM) processes (Fig. 1), were used to fabricate pure Ti, Ti–10W, and Ti–7.5TiC–7.5W (hereafter, all compositions are given in weight percent unless stated otherwise) and the results were compared. For promotion of W dissolution, W powder with a particle size less than 1 μm was used, whereas to achieve the enhanced effect of wear resistance, TiC powder with a relatively larger particle size (1–5 μm) was used (Deshpande et al., 2006). Ti–10W, and Ti–7.5TiC–7.5W powder blends were prepared by mixing the W and TiC powders with commercially pure Ti powders (<150 μm) for more than 30 min in a mixing machine (8000-D Mixer Mill, SPEX CertiPrep, Stanmore, UK) prior to carrying out the two different fabrication processes. For the CHIP process, the samples were compacted into billets by cold isostatic pressing at a pressure of 379 MPa. The billets were then vacuum sintered at 1230 °C for 4 h and densified by hot isostatic pressing (HIP) at 900 °C for 2 h at 100 MPa (Frary et al., 2003), followed by slow cooling within the press. For the AM process, the powder blends were densified by a booster press machine (Dongjin Machinery Co., Incheon, Republic of Korea) at room temperature, and the billets were melted using a 190 A arc under argon in a vacuum arc-melting furnace (Ace Vacuum, Republic of Korea).

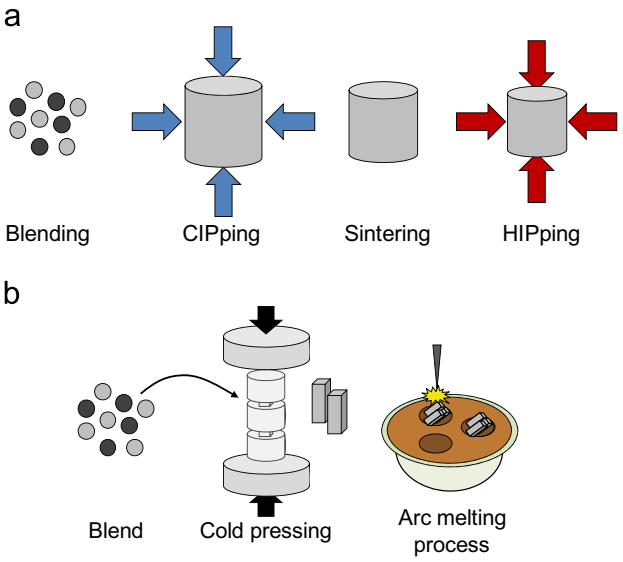

Fig. 1 – Schematic of the two different processing routes: (a) CHIP and (b) AM.

2.2. Mechanical tests

The microstructure of the Ti, Ti–10W, and Ti–7.5TiC–7.5W samples was observed by an optical microscope (Olympus, Tokyo, Japan) on polished cross sections obtained by grinding on SiC papers, polishing with a diamond suspension, and etching for 4–5 s with Kroll's reagent (5% nitric acid, 10% hydrofluoric acid, and 85% water). *Macrohardness* was evaluated using a standard Rockwell hardness testing machine (Mitutoyo, Japan) by applying a 1.6 mm diameter steel ball with a 100 kg major load for Rockwell hardness scale B (HRB). The *microhardness* of the matrix was measured with a Vickers hardness tester (Mitutoyo, Tsukuba, Japan) using a 100–300 g load and an indent time of ~10 s.

A nanomechanical test instrument (Hysitron, USA) was used to carry out nano-scratch tests, which were performed using forces of 300 μN for durations of 20 cycles. The indenter was loaded, forced to scratch the surface of the specimen by

being pulled back and forth for the required number of cycles, and then unloaded. Wear tests were performed using a pin-on-disk tester. Prior to the wear test, all specimens were ground down to 1 μm, cleaned with ethanol, and dried. Round specimens with a diameter of 23 mm were loaded and slid against an abrasive Al_2O_3 counterpart ball (Samhwa Ceramics, Republic of Korea; purity: 93%; Mohs hardness number: 9) at a sliding speed of 0.1 m/s. The applied normal load was fixed at 20 N and the total sliding distance traveled by the ball ranged from 300 to 2000 m. The mass losses of the specimens were measured on an analytical balance with an accuracy of 10^{-4} g.

2.3. *Biocompatibility tests*

CHIP-processed Ti, Ti–10W, and Ti–7.5TiC–7.5W specimens of 3.5 mm square and 2 mm in thickness were used for all the biocompatibility tests, that is, contact angle measurements, cell culturing, and microculture tetrazolium test (MTT), water soluble tetrazolium (WST-1), and extract tests. This is because both the CHIP and AM processes were expected to result in the same composition and similar microstructure, and any possible negative effect of an undissolved W phase on the biocompatibility of the samples could be assessed more easily on the surfaces of the CHIP-processed samples.

Contact-angle measurements were carried out using a contact-angle meter (CAM-PLUS, Tantec Inc., Schaumburg, IL, USA) equipped with a video-imaging system using sessile distilled water drops. The distilled water drops (volume 5 μL) were placed on each specimen surface at ambient temperature. The contact values were then calculated by determining the drop height and diameter using a drop shape analysis program.

For MTT assay, human osteoblast cells obtained from American Type Culture Collection (ATCC, USA) were thawed from frozen stock and routinely subcultured in equal mixtures of Ham's F12 medium and Dulbecco's modified eagle medium (DMEM, Gibco, Invitrogen Corp., Grand Island, NY, USA) containing 0.3 mg/mL of G4180 gentamicin and 10% fetal bovine serum (FBS) at 37 °C in a humidified 5% CO_2 atmosphere. The culture mediums were replaced approximately twice a week. The osteoblast cells were subcultured and harvested following trypsin treatment [0.25% (w/v) trypsin–0.53 mM ethylenediamine-*N*,*N*,*N*′,*N*′-tetraacetic acid, EDTA]. The cells were then seeded onto the surfaces of the Ti, Ti–10W, and Ti–7.5TiC–7.5W specimens with a defined cell density of 2×10^4 cells per well of 48-well microplate with 0.5 mL of the medium. After the subcultured cells were seeded on the specimens, MTT analysis [3-(4,5-dimethylthiazol-2-yl)-2,5-diphenyltetrazolium bromide, Amresco] was used to examine the proliferation of the cells at 1, 3, and 7 d. An MTT solution (50 μL, 5 mg/mL) was added to the medium in the well, which was then maintained in an incubator for 4 h. Upon the formation of crystallized purple-colored formazan dye in the living cells, the specimens were moved to a new microplate and mixed with a 500 μL solution of dimethyl sulfoxide for 30 min. Finally, 100 μL of dissolved purple-colored formazan was placed in 96-well plates and the absorbance of the colored solution was quantified using an enzyme-linked immunosorbent assay (ELISA) plate reader (E-max, Molecular Device, USA) at a wavelength of 570 nm.

WST-1 assay, one of the variations of MTT assay, was performed with mouse fibroblast L929, which had been obtained from ATCC as ATCC CCL1 (NCTC clone 929). This cell line is one of those recommended in ISO 10993-5 (Biological evaluation of medical devices – Part 5: Tests for in vitro cytotoxicity). L929 was subcultured in Eagle's minimum essential medium (EMEM, Nissui, Japan) supplemented with 10% FBS (EMEM+FBS) at 37 °C in a humidified 5% CO_2 atmosphere. Cells were harvested prior to confluence by enzyme solution with 0.1% (w/v) trypsin and 0.02% (w/v) ethylenediamine-*N*,*N*,*N*′,*N*′-tetraacetic acid, disodium salt, dihydrate (EDTA-2Na) in Dulbecco's phosphate buffered saline [PBS(-)], and were seeded onto the surfaces of Ti, Ti-10W, and Ti-7.5TiC-7.5W specimens, which were sterilized at 120 °C for 30 min in a glass dish by autoclaving with drying (SD-321, Tomy) for 1 h and placed separately into a well of 48-well microplate in advance. Seeding condition, which was decided by a pre-test, was 4×10^3 cells per well with 0.5 mL of the EMEM+FBS (w/o phenol red). Upon one, two, and three days of incubation, each sample was moved to a new well of 48-well microplate containing 450 μL of EMEM+FBS (w/o phenol red), and 50 μL of WST-1 solution [a mixture of 2-(4-iodophenyl)-3-(4-nitrophenyl)-5-(2,4-disulfophenyl)-2*H*-tetrazolium, monosodium salt, (Dojindo Laboratories, Japan) and 1-methoxy-5-methylphenazinium methylsulfate (Dojindo Laboratories, Japan)]. The microplate was then maintained in the CO_2 incubator for 4 h. After this secondary incubation, a 200 μL portion of the supernatant was transferred to a 96-well assay plate. The absorbance of the supernatants was measured at 450 nm by a microplate reader (a Multiskan FC Microplate Photometer, Thermo Scientific, USA). The cells in each specimen were fixed for 10 min with a 25% glutaraldehyde solution in the well with the remaining culture medium. They were then stained with 10% (v/v) Giemsa's staining solution diluted with ultrapure water for 15 min to facilitate observation by a microscope. Experiments were performed in duplicate.

Additionally, extraction tests were also performed using L929 mouse fibroblast cells. The extracts of Ti, Ti–10W, and Ti7.5TiC7.5W were prepared by adding EMEM+FBS to each sample at the ratio of 0.1 g/mL, and placed in a CO_2-incubator for 24 h. L929 cells were seeded on a 24-well microplate at a density of 50 cells per well in 0.5 mL of EMEM+FBS. After 24 h of incubation in a CO_2 incubator, the medium was replaced by the next extract or diluted by EMEM+FBS to be 50%. The 24-well microplate was then maintained in a CO_2 incubator for 144 h. The colonies formed were fixed with a 25% glutaraldehyde solution and stained with a 10% (v/v) Giemsa's staining solution. The number of stained colonies on each well was subsequently counted to estimate the relative plating efficiency. Experiments were performed in triplicate.

3. Results and discussion

3.1. *Processing and microstructure*

Fig. 2(a–d) shows micrographs of etched cross sections of the Ti–10W and Ti–7.5TiC–7.5W specimens produced by CHIP and

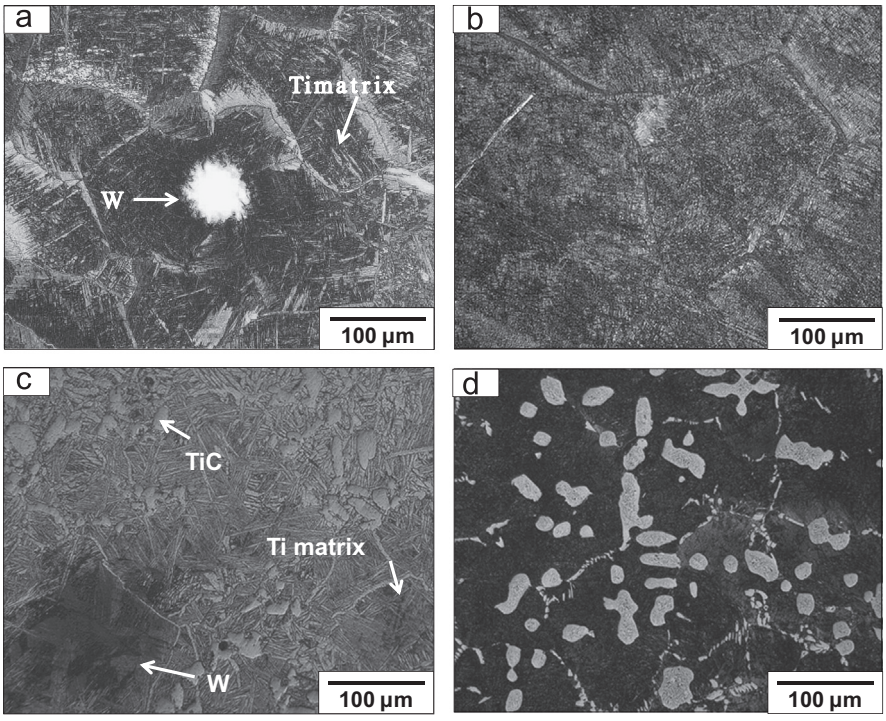

Fig. 2 – Optical micrographs of etched microstructures of (a, b) Ti–10W and (c, d) Ti–7.5TiC–7.5W. (a, c) are microstructures of the materials fabricated by CHIP and (b, d) by AM.

Table 1 – Macrohardness and matrix microhardness.

Material	CHIP processing route		AM processing route	
	Macrohardness (HRB)	Microhardness (HV)	Macrohardness (HRB)	Microhardness (HV)
Pure Ti	78.4±2.9	165.0±10.2	104.6±1.6	317.0±30.5
Ti–10W	106.1±1.5	305.2±14.5	116.8±0.2	415.2±8.9
Ti–7.5TiC–7.5W	102.9±0.5	252.4±15.9	113.7±0.9	361.7±25.6

AM processes, respectively. When alloyed with W, the etched Ti matrix shows an acicular structure due to the dissolution of W in the Ti matrix, which was previously reported and identified as a Widmanstätten α/β structure, with most of the W segregated in the β phase (Frary et al., 2003; Choe et al., 2005a, 2005b). The dissolution of W was anticipated to be fairly complete in the Ti–10W alloy fabricated by CHIP (Fig. 2a), given the W mean particle size of less than 1 μm (Frary et al., 2003; Choe et al., 2005a). However, the degree of W dissolution was expected to be greater in the Ti–10W alloy fabricated by AM (Fig. 2b) owing to the nature of the liquid-state processing. Partially dissolved W particles of distinctive size, which were surrounded by a dark-etched matrix shell corresponding to a diffusion zone with high W content, were rarely observed in either the Ti–10W alloy or the Ti–7.5TiC–7.5W composite fabricated by CHIP, suggesting nearly as complete W dissolution in the Ti matrix of samples processed by CHIP as in those by AM. Relative density of the samples was estimated from the volume percent of porosity measured using image analysis. The relative density of the samples ranged from ~98.1 to 98.7%. Although the image analysis method tends to provide slightly higher relative density values than the Archimedes method (Cho et al., 2012), it is still concluded that both CHIP and AM fabrication processes could produce fairly dense Ti-based composite materials.

3.2. *Mechanical properties*

We have used both Vickers and Rockwell hardness measurements to measure and compare hardness of the samples on both 'micro' and 'macro' scales, respectively. Vickers hardness was used to measure the matrix hardness in the sample, whereas Rockwell hardness was used to measure the hardness of the average microstructure in the entire sample. Table 1 displays and compares the macrohardness (Rockwell) and microhardness (Vickers) values for the samples produced by both CHIP and AM processes. Overall, hardness values are higher for the samples produced by AM than for the samples produced by CHIP. This is most likely due to the inclusion of oxygen in the samples produced by AM. The hardness and strength of Ti and its alloys is considerably affected by oxygen content; for example, the literature hardness value of a commercially pure Ti (CP-Ti) ranges from 147 to 210 HV (Faria et al., 2011; Das et al.,2014; Frary et al., 2003), but the hardness of oxygen content of only 0.55 wt% can increase the hardness of the CP-Ti up to some

300 HV (Donachie, 2000). In particular, the macrohardness of the Ti–10W and Ti–7.5TiC–7.5W specimens produced by CHIP was 106.1±1.5 and 102.9±0.5 HRB (Table 1), respectively, which are approximately 33–35% higher than that of Ti (78.4±2.9 HRB) because of the strengthening effect of the addition of W and TiC, as expected. The macrohardness of the Ti–10W specimen was slightly higher than that of the Ti–7.5TiC–7.5W specimen. This is somewhat counterintuitive because the high hardness of TiC ceramic particles was expected to increase the macrohardness of the Ti–7.5TiC–7.5W composite. These unexpected results were perhaps due to more effective W solid-solution strengthening in the Ti–10W alloy than in the Ti–7.5TiC–7.5W composite. The presence of TiC particles appears to have caused less dissolution of W in the Ti matrix and thus may have reduced the solid-solution strengthening effect of W in the Ti matrix (Choe et al., 2008).

In addition, microscale Vickers hardness (microhardness) tests were carried out to measure the matrix hardness of the specimens. The microhardness values of the Ti, Ti–10W, and Ti–7.5TiC–7.5W specimens produced by CHIP were 165.0±10.2, 305.2±14.5, and 252.4±15.9 HV, respectively (Table 1). The matrix hardness value of 165 HV for the pure Ti specimen agrees well with those reported for CP-Ti (147–210 HV, (Faria et al., 2011; Das et al., 2014; Frary et al., 2003). Although the results show a trend similar to that of the Rockwell hardness values, the matrix hardness of the Ti–10W specimen was considerably higher than that of the Ti–7.5TiC–7.5W specimen. This may be attributed to two reasons. First, the W content used in the Ti–10W specimen was higher than that used in the Ti–7.5TiC–7.5W specimen, possibly resulting in the greater a solid-solution strengthening effect for the Ti–10W specimen. Second, the presence of TiC particles disturbed the dissolution of W into the matrix, as described earlier, which resulted in further reduction of the W solid-solution strengthening effect. According to a previous study (Choe et al., 2008), the microhardness of a Ti–TiC–W composite substantially decreased with increasing TiC composition.

For biomedical applications, a material's wear resistance is important not only for its mechanical stability but also for its biocompatibility because wear and the resultant creation of wear debris particles has been known to be a dominant factor limiting the implant material's long-term usage (Thomas et al., 2012). Fig. 3(a) displays the wear mass loss after the wear test under a load of 20 N for 300–2000 m carried out on the Ti, Ti–10W, and Ti–7.5TiC–7.5W specimens produced by AM. We carried out both wear and nano-scratch tests and compared the results only on AM-processed samples, because dimensions of only those samples were sufficiently large for the pin-on-disk wear test to be conducted. The wear mass loss increased as expected with increasing sliding distance for all tested specimens. Both the Ti–10W and Ti–7.5W–7.5TiC specimens showed significantly lower wear mass losses than pure Ti because the reinforced alloy and composite can sustain higher loads with less plastic deformation (Wu et al., 2005). In other words, solid-solution of W and distribution of reinforcing TiC particles could reduce the plastic deformation of the Ti matrix, and hence, lessened the wear mass loss (Tu et al., 1998). On the other hand, essentially no difference was observed between the wear mass losses of the Ti–10W and Ti–7.5TiC–7.5W specimens, which again is

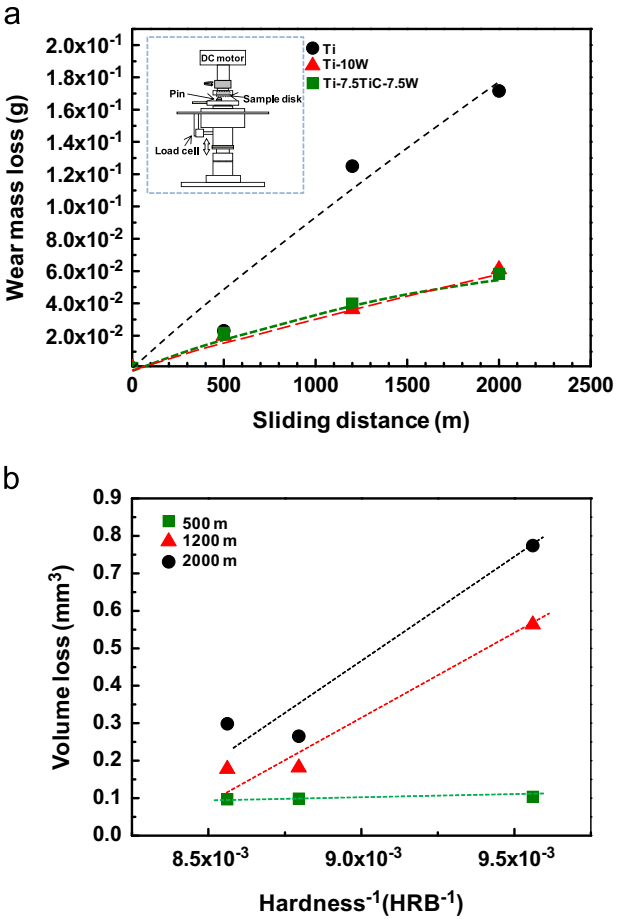

Fig. 3 – Plots of (a) wear mass loss as a function of sliding distance and (b) volume loss as a function of inverse Rockwell hardness for pure Ti, Ti–10W, and Ti–7.5TiC–7.5W. Shown in the inset of (a) is a schematic of the pin-on-disk wear test used in this study.

somewhat counterintuitive because the well-dispersed TiC particles could have resulted in a further reduction in the wear mass loss by hindering dislocation motion and plastic deformation efficiently in the Ti matrix. The strong effect of well-dispersed TiC particles on wear resistance appears to be offset by the reduced dissolution of W, leading to less hardening in the Ti–7.5TiC–7.5W matrix. This is also supported by the nano-scratch results presented in Fig. 4. The Ti–10W alloy showed clearly further improved scratch resistance (scratch depth ~10.43 nm) as compared to the Ti–7.5TiC–7.5W specimen (scratch depth ~16.50 nm), again, most probably due to the enhanced effect of the solid-solution strengthening of W in the Ti matrix.

The effect of hardness on the wear resistance is often described using Archard's law (ASTM E8-03, 1994), which states that the wear volume loss tends to have an inverse relationship with hardness. Despite having an insufficient number of data points to make a firm conclusion, the Ti-based materials studied in this paper indeed tended to follow Archard's inverse relationship between the wear volume loss and hardness, as shown in Fig. 3(b). A less apparent inverse relationship is seen immediately after the shorter sliding distance of 500 m. This is perhaps because during the initial stage of abrasive wear with several hundreds of meters of sliding distance, the abrasive wear

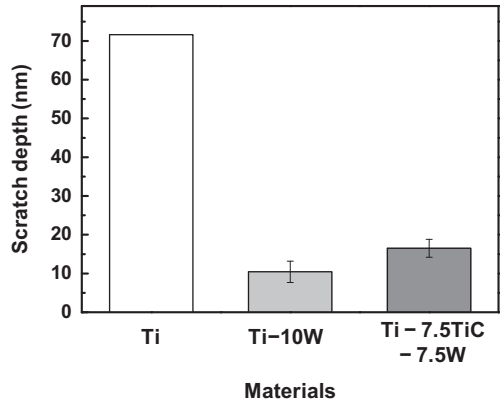

Fig. 4 – Comparison of nano-scratch depth of pure Ti, Ti–10W, and Ti–7.5TiC–7.5W. The test was performed only on the matrix at 300 μN for 20 cycles.

behavior did not reach a steady state, particularly taking into account the relatively high surface roughness of the specimen (1 μm) (Suh et al., 2008). This initially unsteady wear behavior is normally represented by an unstable and irregular value of the initial frictional coefficient (Hong et al., 2011).

Fig. 5 shows SEM images of representative worn surfaces for the Ti–10W alloy after the wear test with a sliding distance of 1200 m. Wear grooves with occasional micro-cracks are observed on the worn surface of the Ti–10W specimen [Fig. 5(a)]. The overall wear behavior of the Ti–10W alloy appears to be that of plastic deformation by plowing and ductile flow of the Ti matrix, which is the typical major wear mechanism for metallic materials (Jain et al., 2010). The presence of grooves and scratches on the worn surfaces evidenced in Fig. 5(a) and (b) indeed supports this plowing wear mechanism. On the other hand, the possible engagement of oxidative wear must not be excluded in this case. In highly reactive metals such as Ti, the formation of TiO_2 on the worn surface is reported to influence the wear behavior of the matrix (Jain et al., 2010). Indeed, energy dispersive X-ray spectroscopic (EDS) analysis on the dotted area of the flake on the Ti matrix shown in Fig. 5(b) shows an unusually high amount of oxygen (ca. 15 wt%), revealing the significant possibility of oxidative wear. In understanding the wear behavior of the Ti–7.5TiC–7.5W specimen, the interfacial bond strength between the TiC particles and the matrix is an important factor to be considered because a relatively weak interfacial bond can cause the reinforcement particles to be pulled out, thus reducing wear resistance (Sandt, 1986; Aziz-Kerrzo, 2011). According to SEM images of the Ti–7.5TiC–7.5W specimen after the wear test, no trace of TiC particle pull-out was observed, suggesting sufficiently good bonding between the TiC particles and matrix.

Although this study finds the overall tribological properties of the Ti–10W and Ti–7.5TiC–7.5W specimens highly suitable for use in biomedical applications, it is desirable for their moduli (80–130 GPa (Ashby and Jones, 1987)) to be further reduced to better match that of natural bone (~40 GPa (Wang et al., 2013)) in order to completely remove the stress-shielding effect, which is caused by the difference between the moduli of the foreign implant and that of natural bone.

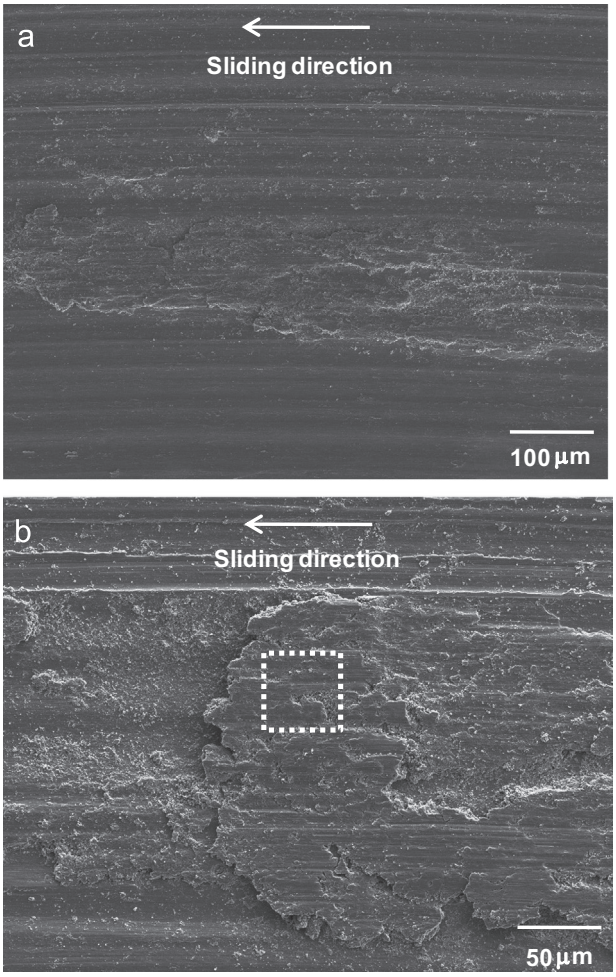

Fig. 5 – SEM images of worn surfaces of the Ti–10W alloy both at (a) lower and (b) higher magnifications. The dotted square shown in (b) is the selected worn area for EDS analysis.

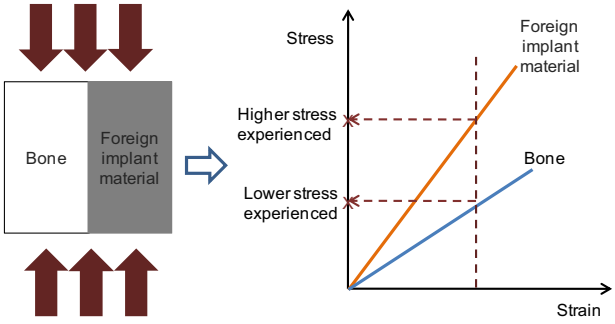

Fig. 6 – Schematic explanation of a stress-shielding effect caused by a large difference between the modulus of the foreign implant and that of natural bone, resulting in degradation or osteoporosis of the bone.

Indeed, the presence of the stress-shielding effect can cause a serious setback in that the external load cannot be transferred appropriately to the bone and is then supported mainly by the implant material, eventually causing either degradation and fracture or osteoporosis of the bone, as shown schematically in Fig. 6. In order to match the modulus

of the foreign implant material to that of natural bone, one can suggest employing Ti–10W and Ti–7.5TiC–7.5W composite foams by modifying conventional powder-metallurgy or space-holder foaming methods (Dunand, 2004). This, however, can only be achieved with some sacrifice of tribological and mechanical properties such as strength, hardness, and wear resistance.

3.3. *Biocompatibility*

Fig. 7 shows the water contact angles of the Ti, Ti–10W, and Ti–7.5TiC–7.5W specimens. The mean contact angles of the Ti, Ti–10W, and Ti–7.5TiC–7.5W specimens were 65 ± 4, 66 ± 6, and $69\pm1^{\circ}$, respectively, with the contact angle of the Ti–7.5TiC–7.5W being slightly higher than those of the other two. However, the three samples showed similar values within an acceptable error range and a somewhat similar tendency towards hydrophilicity for cell culturing and proliferation.

Human osteoblast cell proliferation was examined using MTT assay on the Ti, Ti–10W, and Ti–7.5TiC–7.5W specimens. Fig. 8 shows the relative cell proliferation activity of the osteoblast cells through an MTT assay using the absorbance in 1, 3, and 7 d after the cells were seeded onto the samples. With increasing time, a noticeable increase in cell proliferation was observed in all three samples. A more significant increase in the absorbance occurred between 1 d and 3 d than between 3 d and 7 d for all three samples. In addition, the most pronounced increase was observed in Ti–10W from 0.083 at 1 d to 0.113 at 7 d, with a 73.1% increase in absorbance. On the other hand, no distinguishable difference was observed between the three samples at the same incubation time in all three measurements within the statistical error range ($p<0.5$). This good biocompatibility of all three Ti-based samples is perhaps because TiO_2, which has good biocompatibility with living tissue, formed well on all three samples, regardless of the additions of W and TiC.

The mouse fibroblast WST-1 assay test showed similar results, i.e., no significant differences were detected in the cell viability between the three tested samples after 1, 2, and 3 d of proliferation (Fig. 9). As expected, the absorbance value increased near linearly with increasing proliferation time. For example, the mean absorbance values of the Ti, Ti–10W, and Ti–7.5TiC–7.5W specimens ranged between 0.17 and 0.20 after 1 d of incubation, whereas the mean absorbance values of those specimens after 3 d of incubation were significantly higher, ranging between 0.37 and 0.43 (Fig. 9). Similar proliferation trends were observed through optical microscopic images, as shown in Fig. 10, which compares the number and morphology of the L929 cultured on the Ti, Ti–10W, and Ti–7.5TiC–7.5W specimens. The number of cells increased with increasing incubation time from 1 d to 3 d, with no significant difference between the Ti, Ti–10W, and Ti–7.5TiC–7.5W specimens at the same incubation times (Fig. 10).

We expanded the biocompatibility study by further carrying out extract tests and comparing the relative plating efficiencies of the three samples (Fig. 11). The relative plating efficiency was obtained by calculating the ratio of the mean number of the colonies in the extract wells to that in the control wells. As shown in Fig. 11, Ti has a tendency of improved relative plating efficiency with decreasing extract concentration from 100% to 50%, but both Ti-10W and Ti-7.5TiC-7.5W do not show clear dependence on their extract concentrations. Additionally, no statistically considerable difference was observed between the Ti, Ti–10W, and Ti–

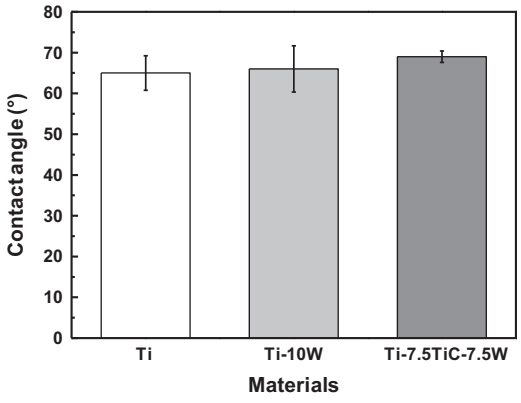

Fig. 7 – Contact angles of Ti, Ti–10W, and Ti–7.5TiC–7.5W.

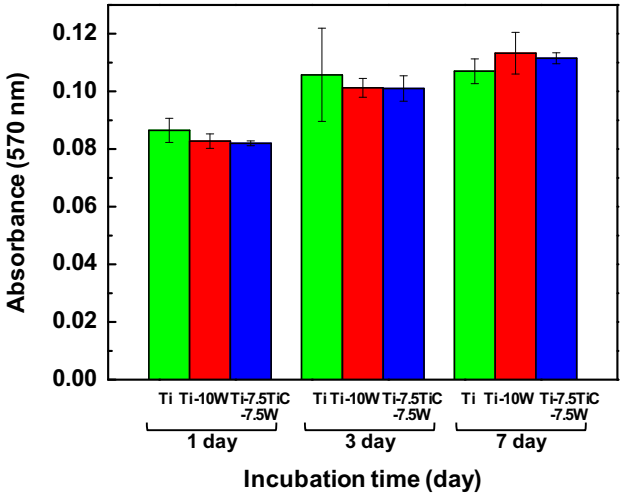

Fig. 8 – Cell proliferation of human osteoblasts on Ti, Ti–10W, and Ti–7.5TiC–7.5W examined by MTT assay.

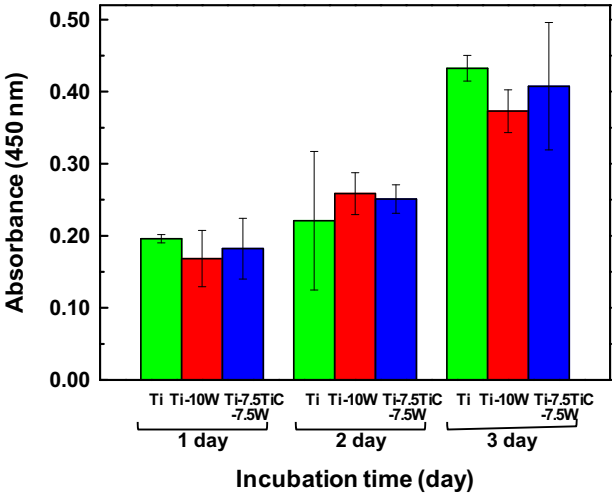

Fig. 9 – Cell proliferation of mouse fibroblasts on Ti, Ti–10W, and Ti–7.5TiC–7.5W examined by WST-1.

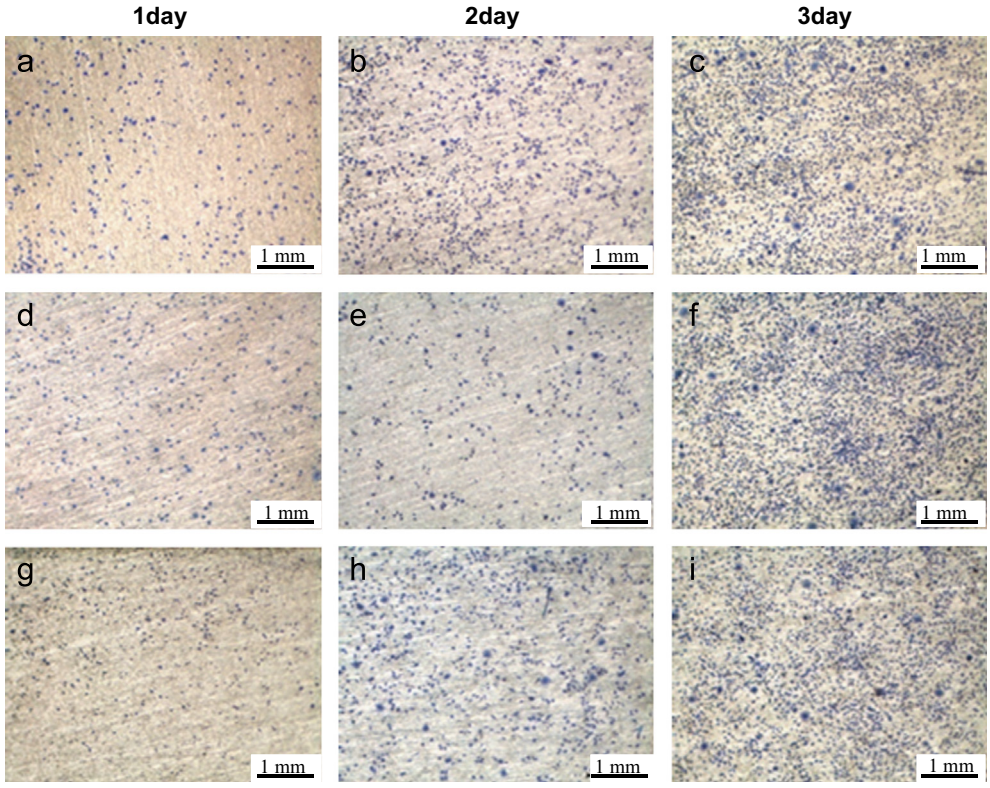

Fig. 10 – Optical images of L929 cells cultured on the specimens of (a, b, c) Ti, (d, e,f) Ti–10W, and (g, h, i) Ti–7.5TiC–7.5W after being dyed with Giemsa's staining solution.

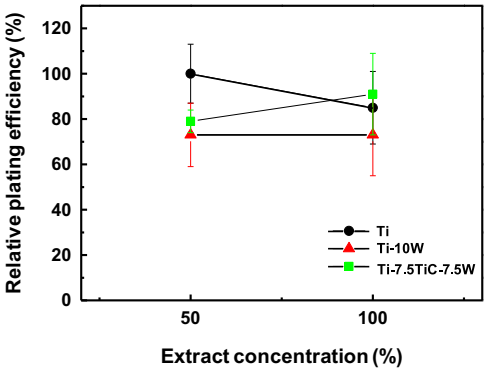

Fig. 11 – Plating efficiencies of L929 cells cultured with the medium extract of Ti, Ti–10W, and Ti–7.5TiC–7.5W.

7.5TiC–7.5W specimens. It was thus confirmed again that none of the three Ti-based materials studied in this paper showed cytotoxicity in L929 mouse fibroblast cells or unacceptable biocompatibility.

4. Conclusions

This study compared the microstructure, biocompatibility, and tribological properties of Ti–10W and Ti–7.5TiC–7.5W composites processed by both CHIP and AM processing methods with those of the control pure Ti. We have shown through macro- and microhardness, nano-scratch, and wear measurements that additions of W and TiC particles to Ti can significantly improve its tribological properties. Furthermore, we have also shown by performing MTT and WST-1 tests, as well as by observing cell morphology on the specimens, that additions of W and TiC particles do not affect the excellent biocompatibility of Ti, and thus these materials are suitable for use in biomedical applications.

Acknowledgments

This research was supported by the Pioneer Research Center Program through the National Research Foundation (NRF) of Korea funded by the Ministry of Education, Science, and Technology (2011-0001684). HC also acknowledges support from the Basic Science Research Program (2010–0005775; 2010–0029106) and the Priority Research Centers Program (2009–0093814) through the National Research Foundation (NRF) of Korea funded by the Ministry of Education, Science, and Technology.

REFERENCES

ASTM E8-03, 1994. Standard Test Methods for Tension Testing of Metallic Materials: Annual book of ASTM standards, ASTM, Philadelphia, PA.

Adell, R., et al., 1970. Intra-osseous anchorage of dental prostheses. Scand. J. Plast. Reconstr. Surg. 4, 19–34.

Ashby, M.F., Jones, D.R.H., 1987. Engineering Materials 1: An Introduction to Their Properties and Applications. Pergamon Press, Oxford.

Aziz-Kerrzo, M., 2011. Electrochemical studies on the stability and corrosion resistance of titanium-based implant materials. Biomaterials 22, 1531–1539.
Brunette, D.M., et al., 2001. Titanium in Medicine: Materials Science, Surface Science, Engineering, Biological Responses and Medical Applications. Springer-Verlag, New York.
Cho, Y.-H., et al., 2012. Mechanical properties of the solid Li-ion conducting electrolyte: $Li_{0.33}La_{0.57}TiO_3$. J. Mater. Sci. 47, 5970–5977.
Choe, H., et al., 2005a. Effect of tungsten additions on the mechanical properties of Ti-6Al-4V. Mater. Sci. Eng. A 396, 99–106.
Choe, H., et al., 2005b. Effect of tungsten dissolution on the mechanical properties of Ti-W composites. J. Alloys Compd. 390, 62–66.
Choe, H., et al., 2008. Mechanical properties of Ti-W alloys reinforced with TiC particles. Mater. Sci. Eng. A 485, 703–710.
Das, M., et al., 2014. In situ synthesized TiB–TiN reinforced Ti6Al4V alloy composite coatings: microstructure, tribological and in-vitro biocompatibility. J. Mech. Behav. Biomed. Mater. 29, 259–271.
Deshpande, P.K., et al., 2006. Infrared processed Cu composites reinforced with WC particles. Mater. Sci. Eng. A 429, 58–65.
Donachie, M.J., 2000. Titanium: A Technical Guide, 2nd ed. ASM International, Metals Park, OH.
Dunand, D.C., 2004. Processing of titanium foams. Adv. Eng. Mater. 6, 369–376.
Enderle, J.J.D., et al., 2005. Introduction to Biomedical Engineering, 2nd ed. Elsevier Academic Press, Burlington, MA.
Faria, A.C.L., et al., 2011. Wear resistance of experimental titanium alloys for dental applications. J. Mech. Behav. Biomed. Mater. 4, 1873–1897.
Feng, B., et al., 2004. Characterization of titanium surfaces with calcium and phosphate and osteoblast adhesion. Biomaterials 25, 3421–3428.
Frank, G.S., 2002. Magnetic resonance safety update 2002: implants and devices. J. Magn. Reson. Imaging 16, 485–496.
Frary, M., et al., 2003. Microstructure and mechanical properties of Ti/W and Ti-6Al-4V/W composites fabricated by powder-metallurgy. Mater. Sci. Eng. A 344, 103–112.
Geetha, M., et al., 2009. Ti based biomaterials, the ultimate choice for orthopaedic implants – a review. Prog. Mater. Sci. 54, 397–425.
Hong, E.J., et al., 2011. Tribological properties of copper alloy-based composites reinforced with tungsten carbide particles. Wear 270, 591–597.
Iijima, D., et al., 2003. Wear properties of Ti and Ti-6Al-7Nb castings for dental prostheses. Biomaterials 24, 1519–1524.
Jain, A., et al., 2010. Grain size-wear rate relationship for titanium in liquid nitrogen environment. Acta Mater. 58, 2313–2323.
Sandt, A., 1986. Coatings applied by thermal spraying and wearing behavior. Schweissen. Schneiden 38, 163–168.
Suh, M.S., et al., 2008. Friction and wear behavior of structural ceramics sliding against zirconia. Wear 264, 800–806.
Temenoff, J.S., Mikos, A.G., 2008. Biomaterials: The Intersection of Biology and Materials Science. Pearson-Prentice Hall, New Jersey.
Thomas, V., et al., 2012. In vitro studies on the effect of particle size on macrophage responses to nanodiamond wear debris. Acta Biomater. 8, 1939–1947.
Tu, J.P., et al., 1998. Friction and wear behavior of Cu-Fe_3Al powder metallurgical composites in dry sliding. Wear 220, 72–79.
Wang, Y.B., et al., 2013. In vitro and in vivo studies on Ti-based bulk metallic glass as potential dental implant material. Mater. Sci. Eng. C 33, 3489–3497.
Wu, T.F., et al., 2005. Effects of tungsten carbide and cobalt particles on corrosion and wear behavior of copper matrix composite. Mater. Sci. Technol. 25, 295–304.